Electronic Supplementary Information

Luminescent heteroleptic Eu(III) probes for the selective detection of diethyl chlorophosphate as G-series nerve agent mimic in the vapor phase using solid-state films

Zafar Abbas,[a] Usha Yadav,[a] Ray J. Butcher,[b] Ashis K. Patra*[a]

[a]Department of Chemistry, Indian Institute of Technology Kanpur, Kanpur 208016, Uttar Pradesh, India

[b]Department of Chemistry, Howard University, Washington DC 20059, USA

Table of Contents

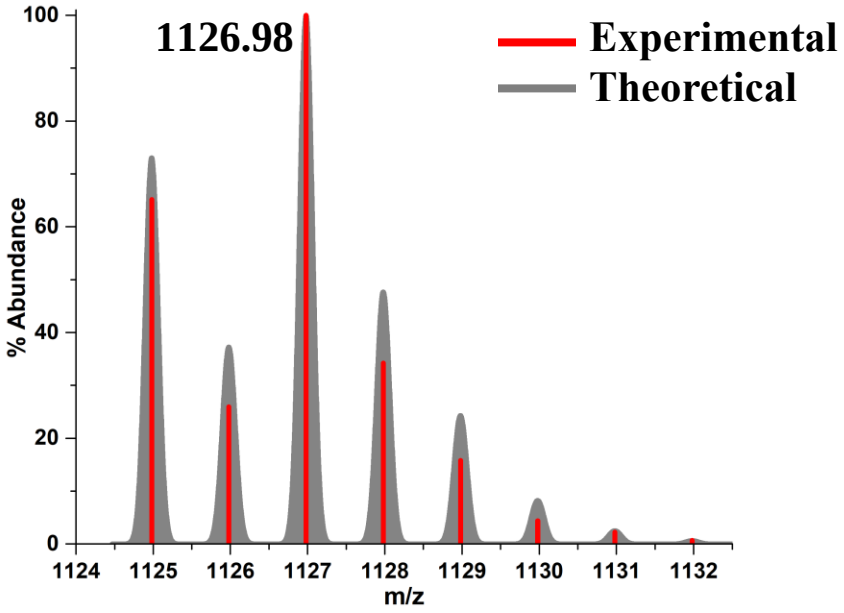

Figure S1. ESI-MS spectra of the **Eu(*o*-OH)** in $CHCl_3$ showing observed molecular ion peak as $[M-H]^-$ at *m/z* 1126.98 with theoretically predicted isotopic distribution profile.

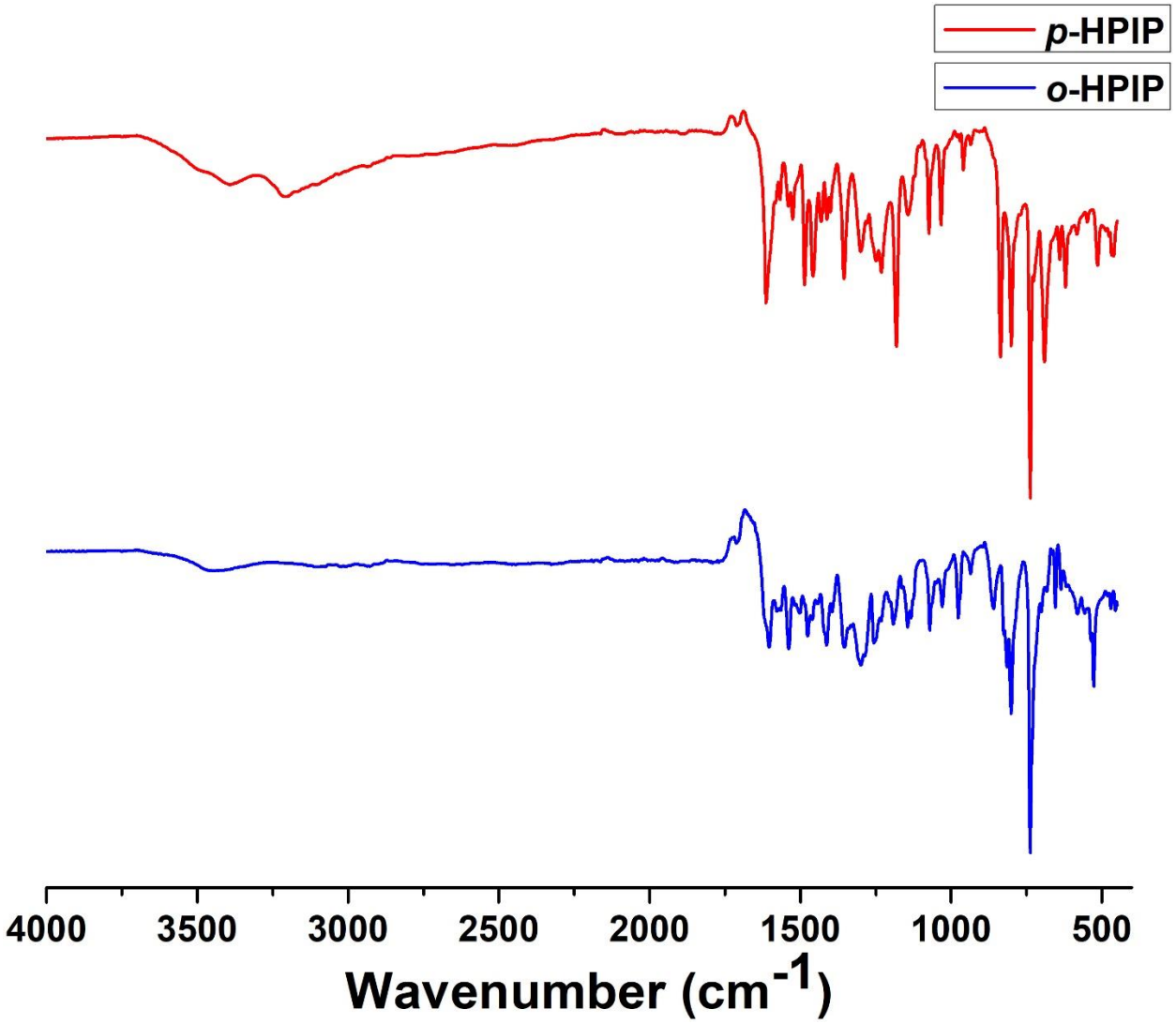

Figure S2. FT-IR spectra of ***o*-HPIP** and ***p*-HPIP** ligands in solid state using KBr disc in the range 400-4000 cm^{-1}.

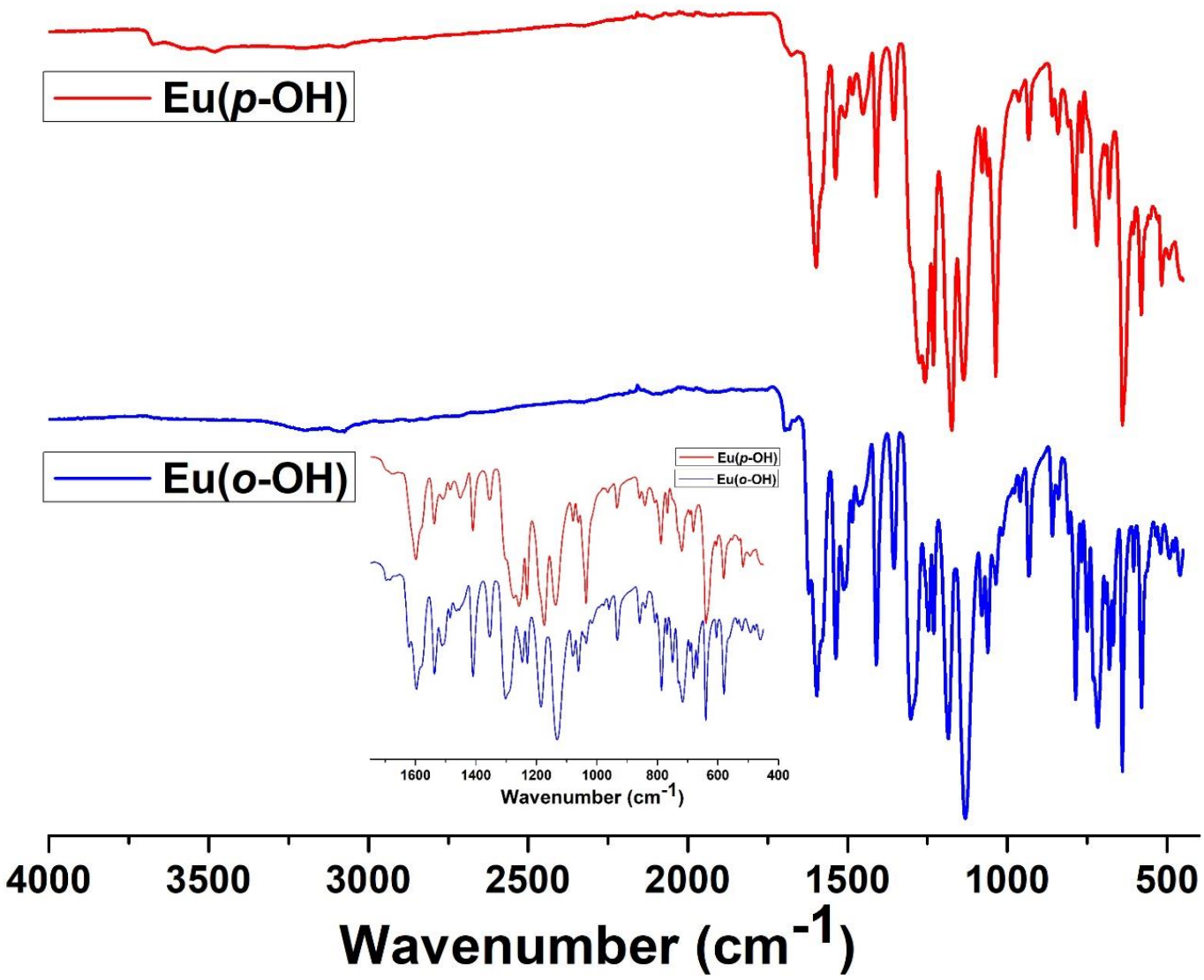

Figure S3. FT-IR spectra of **Eu(*o*-OH)** and **Eu(*p*-OH)** complexes in solid state using KBr disc in the range 400-4000 cm^{-1}. The inset figure shows the overlay of the FT-IR spectra in finger-print region.

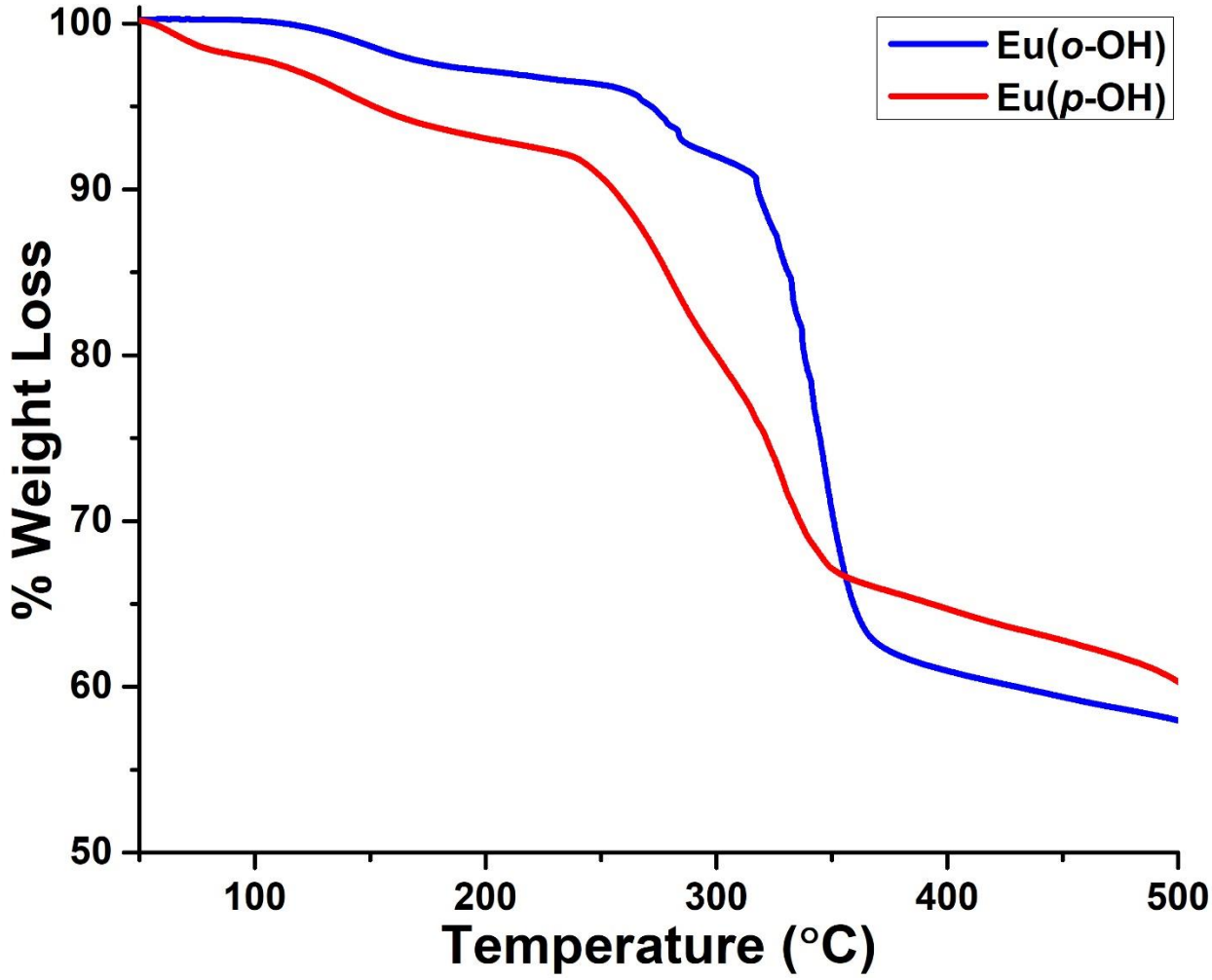

Figure S4. TGA plot of the **Eu(*o*-OH)** and **Eu(*p*-OH)** complexes at a heating rate of 10 °C min^{-1} under N_2 atmosphere.

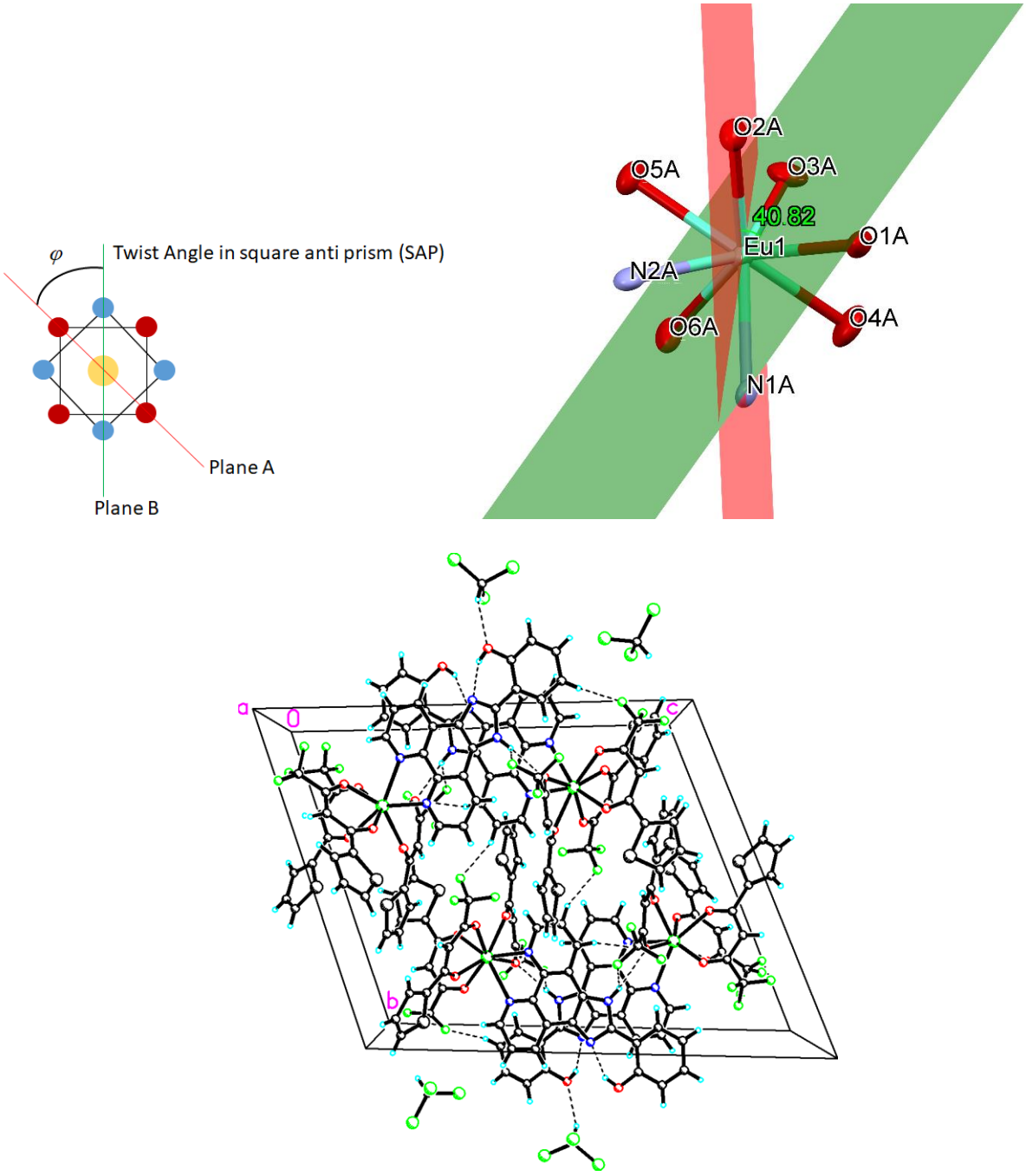

Figure S5. Perspective drawing of the **Eu(*o*-OH)** with twist angle (top) and unit cell packing diagram (bottom) of the **Eu(*o*-OH)** along b-axis.

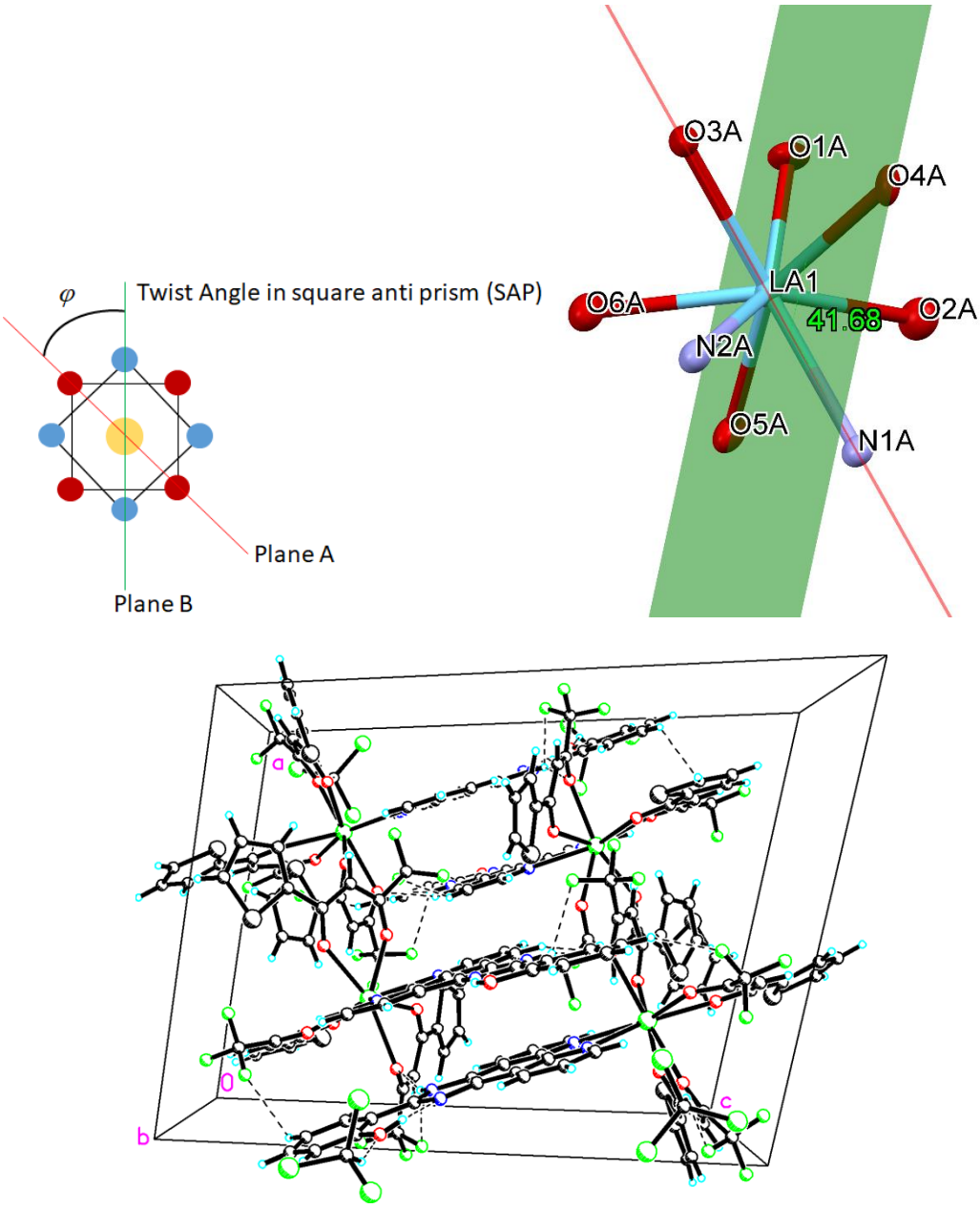

Figure S6. Perspective drawing of the **La(*o*-OH)** with the twist angle (top) and unit cell packing diagram (bottom) of the **La(*o*-OH)** along b-axis.

Table S1. Selected crystallographic data and structure refinement parameters of complexes.

Parameter	**[Eu(*o*-HPIP)(TTA)$_3$]·(CHCl$_3$)**	**[La(*o*-HPIP)(TTA)$_3$]·2(CHCl$_3$)**
Empirical formula	$C_{44}H_{25}Cl_3EuF_9N_4O_7S_3$	$C_{45}H_{26}Cl_6F_9LaN_4O_7S_3$
Formula weight	1247.17	1353.49
Crystal system	Triclinic	Triclinic
Space group	*P*-1	*P*-1
a /Å	15.4707(13)	15.852(3)
b /Å	17.5731(15)	17.886(3)
c /Å	21.2458(18)	21.388(3)
α (deg)	67.219(3)	66.895(4)
β (deg)	76.283(3)	73.584(4)
γ (deg)	73.703(3)	71.157(4)
Volume (Å^3)	5057.4(8)	5193.7(14)
Z	4	4
D_x *(Mg m^{-3})*	1.638	1.731
μ *(mm^{-1})*	1.607	1.338
F(000)	2464	2672
T(K)	100(2)	100(2)
θ range for data collection(deg)	2.988 to 28.266	2.281 to 28.327
Limiting indices	-20≤ h ≤ 20, -23 ≤ k ≤ 23, -28 ≤ l ≤ 28	-21 ≤ h ≤ 21, -23 ≤ k ≤ 23, -28 ≤ l ≤ 28
Reflections collected	80074	71657
Unique reflections	24985	25777
R(int)	0.1393	0.0909
Data/restraint/parameter	24985 / 2059 / 1411	25777 / 1245 / 1651
GOF on F^2	1.106	1.083
R_1[a] and wR_2[b] [$I>2\sigma(I)$]	0.1443 and 0.2783	0.0879 and 0.1696
R_1 and wR_2 (all data)	0.2099 and 0.3108	0.1388 and 0.1912
Largest diff. peak and hole (e.A^{-3})	2.197 and -4.106	2.528 and -1.509
CCDC deposition number	2049309	2049310

[a] $R_1 = \Sigma||F_0| - |F_C||/\sum|F_0|$. [b] $wR_2 = \{\sum[w(F_0^2 - F_C^2)]/\sum[w(F_0^2)^2]\}^{1/2}$.

Table S2. Selected bond lengths [Å] and bond angles [°] for **Eu(*o*-OH)** and **La(*o*-OH)**.			
[Eu(*o*-HPIP)(TTA)$_3$]		**[La(*o*-HPIP)(TTA)$_3$]**	
	Bond Length (Å)		Bond Length (Å)
Eu(1)-O(1A)	2.340(10)	La(1)-O(1A)	2.445(5)
Eu(1)-O(2A)	2.373(9)	La(1)-O(2A)	2.449(5)
Eu(1)-O(3A)	2.375(11)	La(1)-O(6A)	2.457(5)
Eu(1)-O(5A)	2.383(9)	La(1)-O(5A)	2.457(5)
Eu(1)-O(4A)	2.388(10)	La(1)-O(3A)	2.479(5)
Eu(1)-O(6A)	2.413(9)	La(1)-O(4A)	2.531(5)
Eu(1)-N(1A)	2.623(11)	La(1)-N(1A)	2.728(6)
Eu(1)-N(2A)	2.545(12)	La(1)-N(2A)	2.673(6)
	Bond Angles (°)		Bond Angles (°)
O(1A)-Eu(1)-O(2A)	71.1(3)	O(4B)-La(2)-O(1B)	134.12(19)
O(1A)-Eu(1)-O(3A)	98.6(4)	O(4B)-La(2)-O(3B)	69.65(19)
O(2A)-Eu(1)-O(3A)	89.2(3)	O(1B)-La(2)-O(3B)	78.3(2)
O(1A)-Eu(1)-O(5A)	141.8(3)	O(4B)-La(2)-O(5B)	120.16(19)
O(2A)-Eu(1)-O(5A)	71.9(3)	O(1B)-La(2)-O(5B)	78.31(17)
O(3A)-Eu(1)-O(5A)	71.5(4)	O(3B)-La(2)-O(5B)	73.25(19)
O(1A)-Eu(1)-O(4A)	73.3(4)	O(4B)-La(2)-O(2B)	75.48(19)
O(2A)-Eu(1)-O(4A)	136.1(4)	O(1B)-La(2)-O(2B)	70.09(17)
O(3A)-Eu(1)-O(4A)	71.4(4)	O(3B)-La(2)-O(2B)	85.6(2)
O(5A)-Eu(1)-O(4A)	132.0(4)	O(5B)-La(2)-O(2B)	144.98(17)
O(1A)-Eu(1)-O(6A)	146.7(3)	O(4B)-La(2)-O(6B)	77.58(18)
O(2A)-Eu(1)-O(6A)	142.0(3)	O(1B)-La(2)-O(6B)	144.45(17)
O(3A)-Eu(1)-O(6A)	86.9(3)	O(3B)-La(2)-O(6B)	106.2(2)
O(5A)-Eu(1)-O(6A)	71.1(3)	O(5B)-La(2)-O(6B)	69.79(17)
O(4A)-Eu(1)-O(6A)	77.5(4)	O(2B)-La(2)-O(6B)	144.46(16)
O(1A)-Eu(1)-N(2A)	103.5(4)	O(4B)-La(2)-N(1B)	93.04(18)
O(2A)-Eu(1)-N(2A)	73.3(3)	O(1B)-La(2)-N(1B)	108.78(18)
O(3A)-Eu(1)-N(2A)	145.2(4)	O(3B)-La(2)-N(1B)	159.41(19)
O(5A)-Eu(1)-N(2A)	74.5(4)	O(5B)-La(2)-N(1B)	126.66(18)
O(4A)-Eu(1)-N(2A)	140.8(4)	O(2B)-La(2)-N(1B)	79.05(17)
O(6A)-Eu(1)-N(2A)	89.0(3)	O(6B)-La(2)-N(1B)	79.67(16)
O(1A)-Eu(1)-N(1A)	76.3(3)	O(4B)-La(2)-N(2B)	150.52(19)
O(2A)-Eu(1)-N(1A)	116.4(4)	O(1B)-La(2)-N(2B)	71.67(18)
O(3A)-Eu(1)-N(1A)	149.4(3)	O(3B)-La(2)-N(2B)	138.60(19)
O(5A)-Eu(1)-N(1A)	130.2(3)	O(5B)-La(2)-N(2B)	73.32(18)
O(4A)-Eu(1)-N(1A)	78.3(4)	O(2B)-La(2)-N(2B)	109.19(17)
O(6A)-Eu(1)-N(1A)	82.4(3)	O(6B)-La(2)-N(2B)	84.22(17)
N(2A)-Eu(1)-N(1A)	63.4(3)	N(1B)-La(2)-N(2B)	60.70(18)

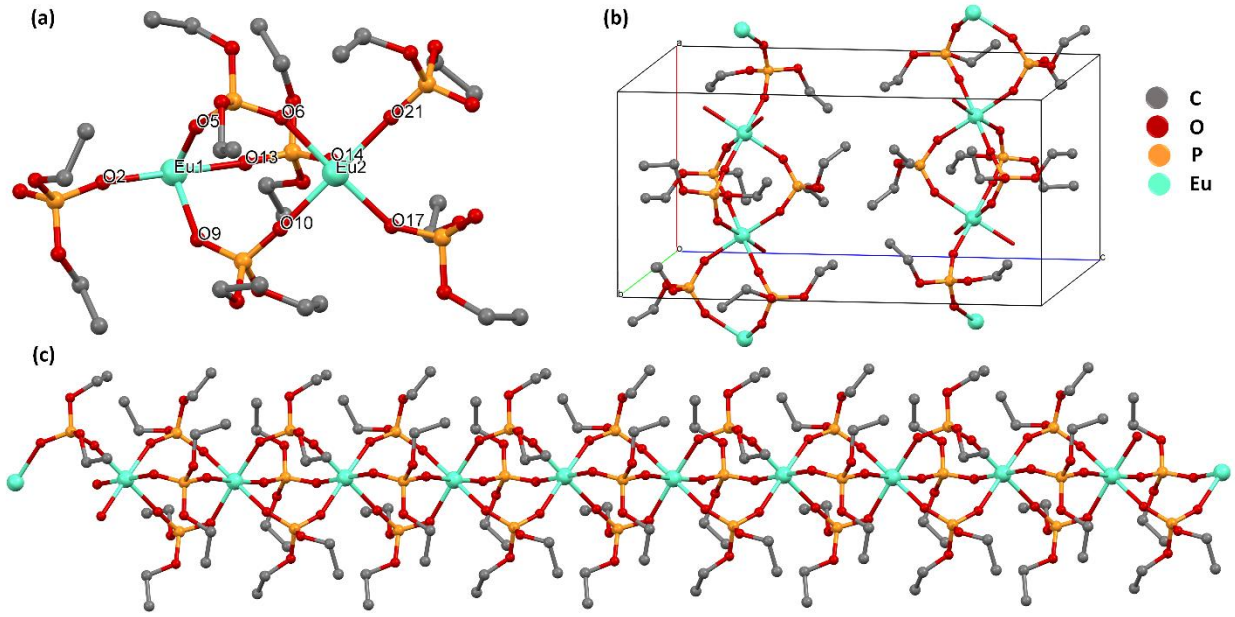

Figure S7. a) Asymmetric unit of $[Eu(DHP)_3]_n$ polymer chain; **b**) Unit cell diagram of the $[Eu(DHP)_3]_n$ structure viewed along b-axis; **c**) A view of the 1-D chain showing Eu(III) ion forming a chain having three bridging DHPs between the two ions. Hydrogen atoms are omitted for clarity.

Table S3. Selected crystallographic data and structure refinement parameters of **Eu(*o*-OH)** and DCP reaction product: $[Eu(DHP)_3]_n$.

Parameters	$[Eu(DHP)_3]_n$
Empirical formula	$C_{24}H_{60}Eu_2O_{24}P_6$
Formula weight	1222.46
Crystal system	Triclinic
Space group	*P*-1
a Å	10.1425(15)
b Å	11.2668(17)
c Å	20.708(3)
α (deg)	101.038(4)
β (deg)	90.599(4)
γ (deg)	91.973(4)
Volume Å^3	2320.8(6)
Z	2
D_x *(Mg m^{-3})*	1.749
μ *(mm^{-1})*	2.960
F(000)	1224
T(K)	100(2)
θ range for data collection(deg)	4.46 to 50.1
Limiting indices	-12≤ h ≤ 12, -13 ≤ k ≤ 13, -24 ≤ l ≤ 24
Reflections collected	24255
Unique reflections	8005
R(int)	0.0619
Data/restraint/parameter	8005 / 0 / 499
GOF on F^2	1.163
R_1[a] and wR_2[b] [I>2σ(I)]	0.0565 and 0.1194
R_1 and wR_2 (all data)	0.0724 and 0.1278
Largest diff. peak and hole (e.A^{-3})	1.96 and -1.58
CCDC deposition number	2069827

[a] $R_1 = \Sigma||F_0| - |F_C||/\Sigma|F_0|$. [b] $wR_2 = \{\sum[w(F_0^2 - F_C^2)]/\sum[w(F_0^2)^2]\}^{1/2}$.

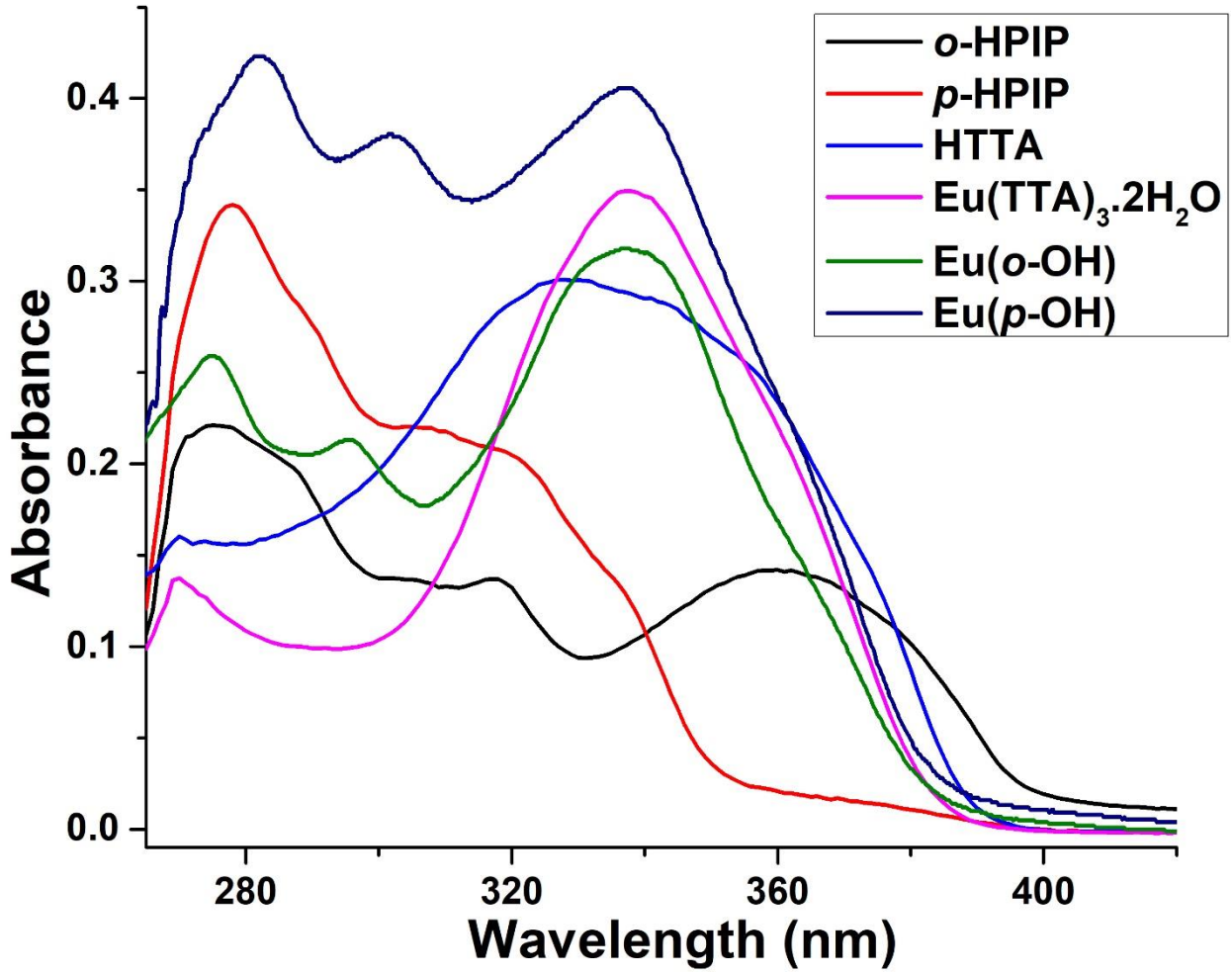

Figure S8. Electronic absorption spectra of the ligands (*o*/*p*-HPIP and TTA) (15 μM), $Eu(TTA)_3.2H_2O$ (5 μM) and complex **Eu(*o*-OH)** and **Eu(*p*-OH)** (5 μM) in MeCN at 298 K.

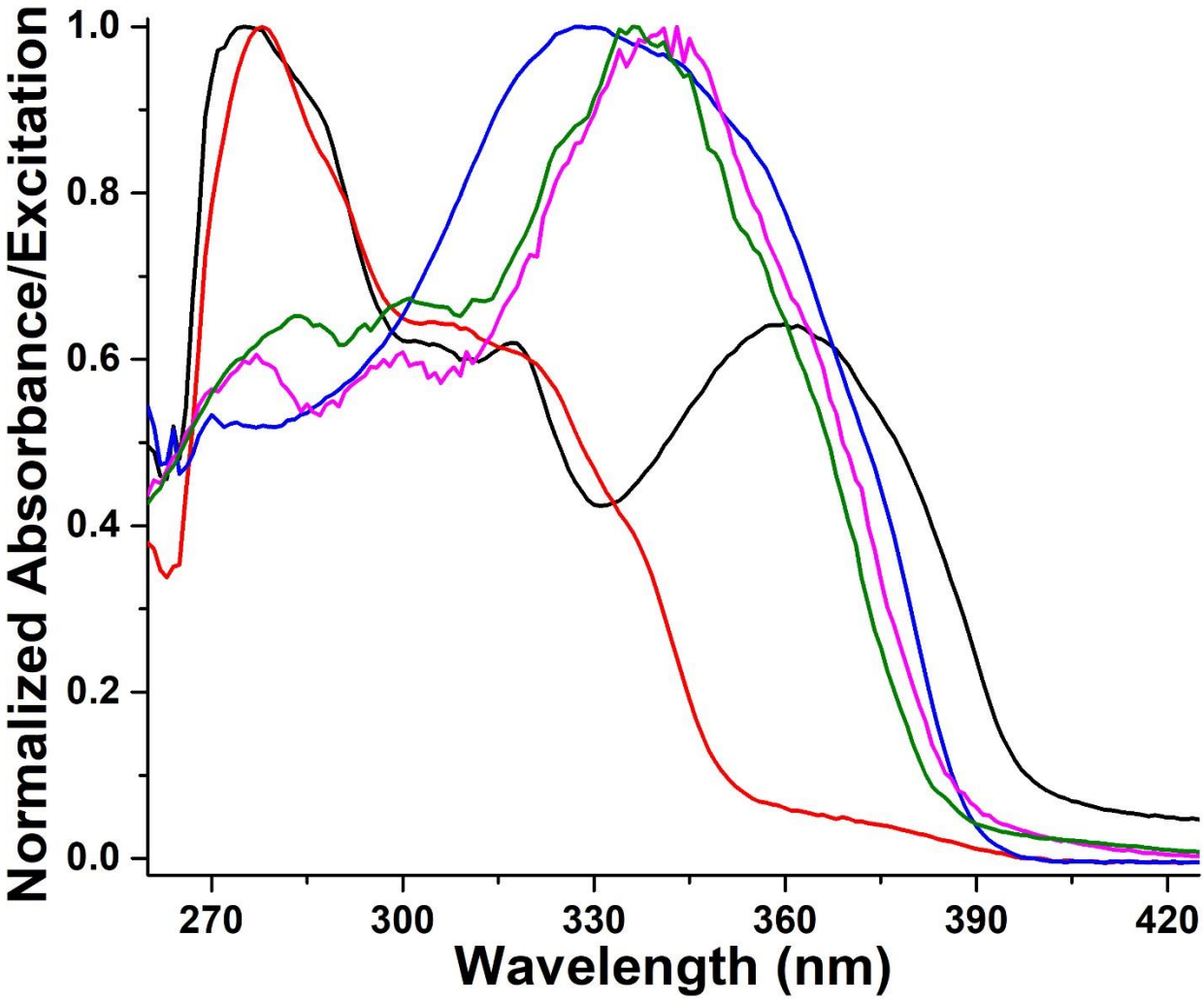

Figure S9. Electronic absorption spectra of the ligands (*o*/*p*-HPIP and TTA) (15 μM) and excitation spectra of the complexes **Eu(*o*-OH)** and **Eu(*p*-OH)** (5 μM) in MeCN at 298 K.

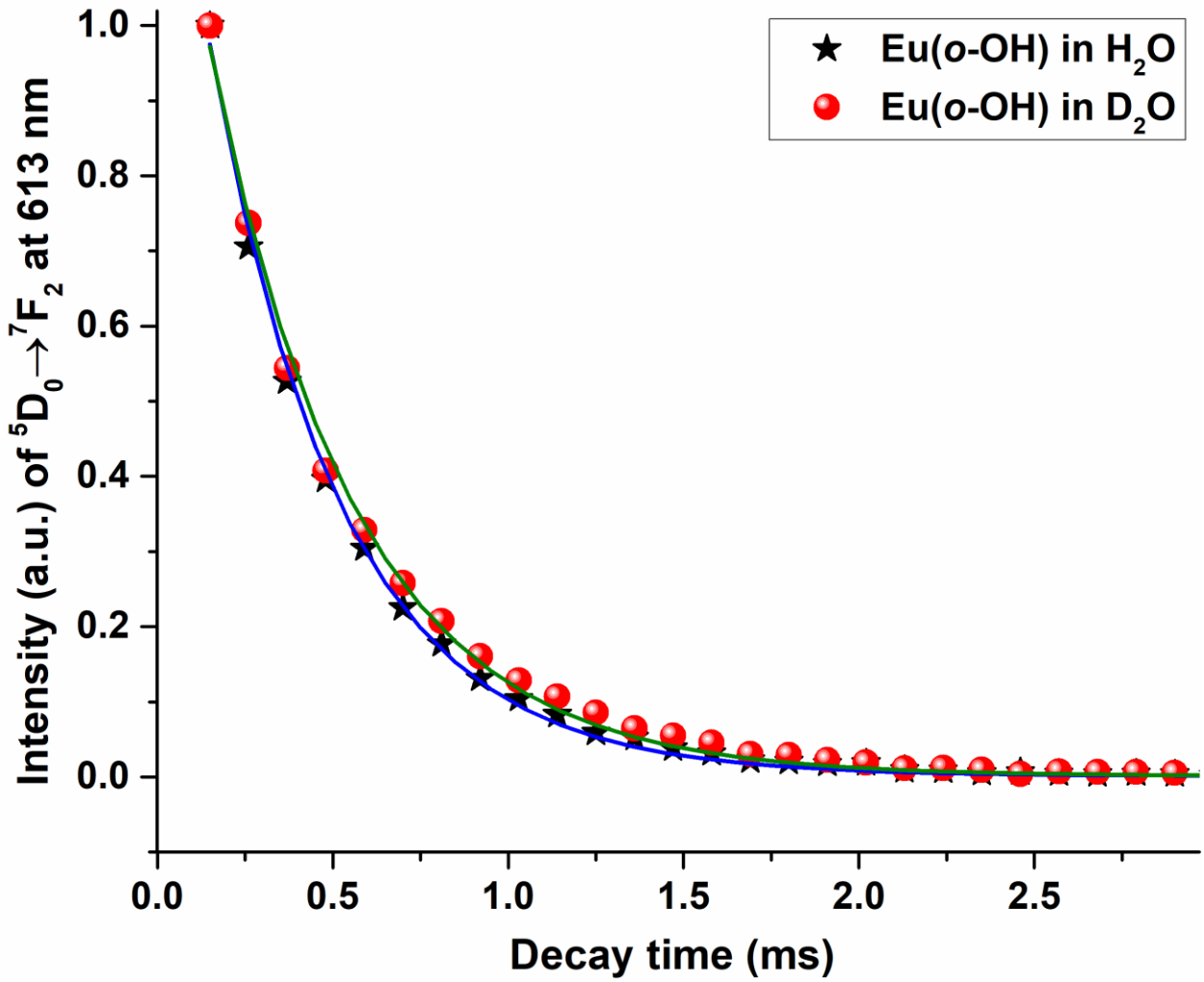

Figure S10. Luminescence decay profile of $^5D_0 \rightarrow {}^7F_2$ transition and lifetime measurements for complex **Eu(*o*-OH)** in H_2O and D_2O (5 μM) at 298 K. λ_{ex}= 340 nm, delay time and gate time = 0.1 ms, total decay time = 10.0 ms, Ex. and Em. Slit width = 5 nm.

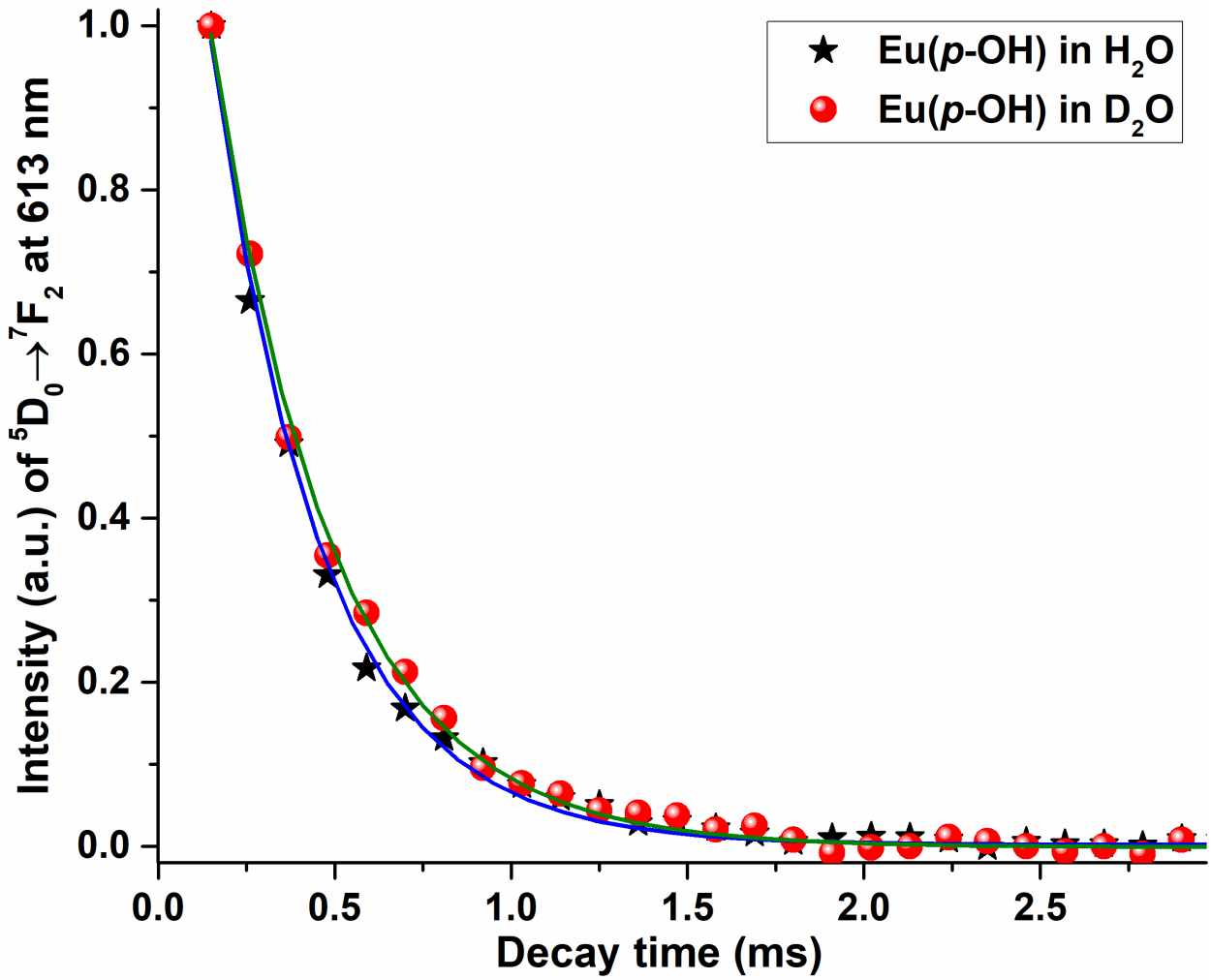

Figure S11. Luminescence decay profile of $^5D_0 \rightarrow {}^7F_2$ transition and lifetime measurements for complex Eu(*p*-OH) in H_2O and D_2O (5 μM) at 298 K. λex= 340 nm, delay time and gate time = 0.1 ms, total decay time = 3.0 ms, Ex. and Em. Slit width = 5 nm.

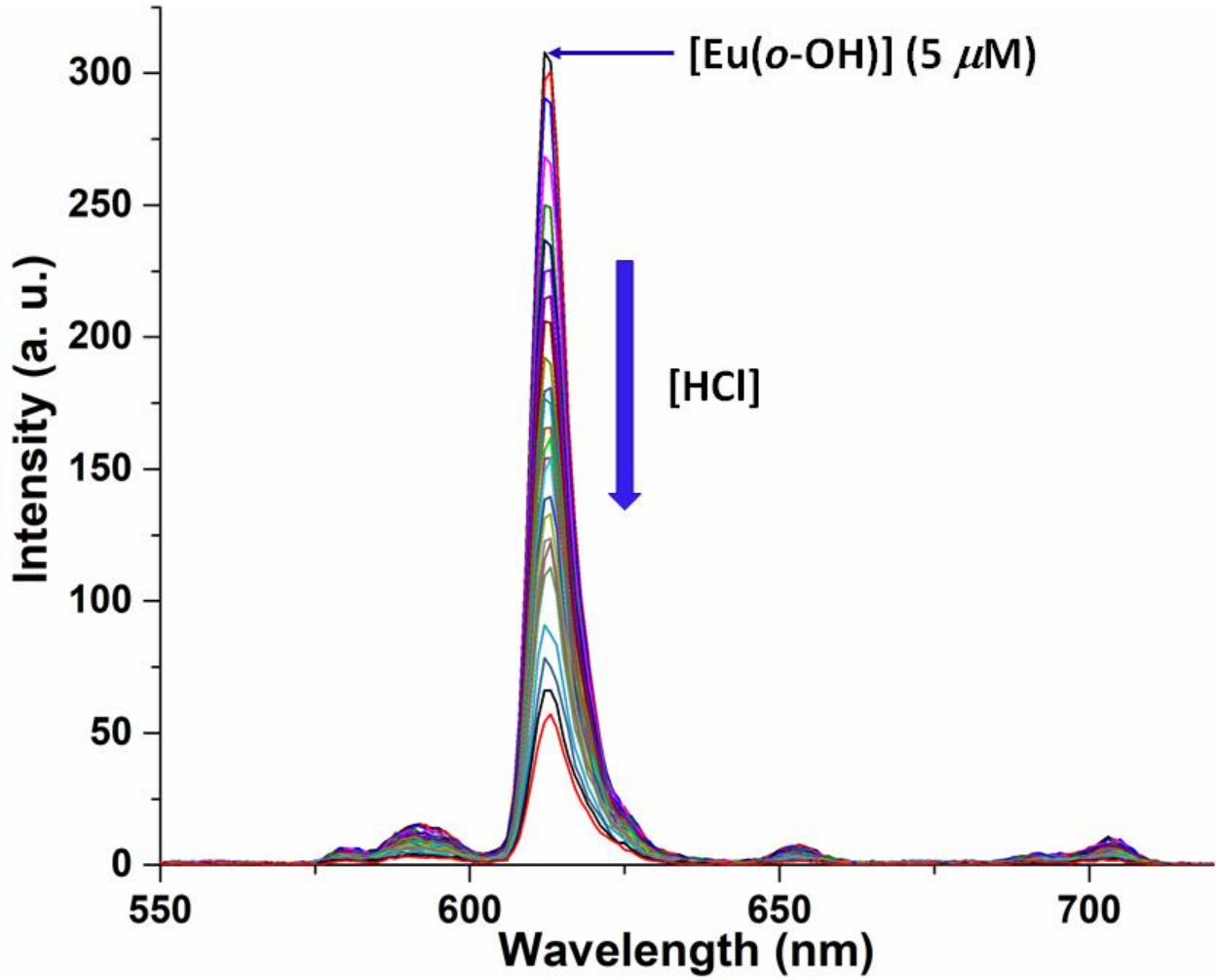

Figure S12. Changes in the PL spectra (λ_{ex} = 340 nm) of **Eu(*o*-OH)** (5 μM) with the increasing concentration of **HCl** (0-30 μM) observed at characteristic emission from the hypersensitive band of Eu(III) ion ($^5D_0 \rightarrow {}^7F_2$ = 613 nm).

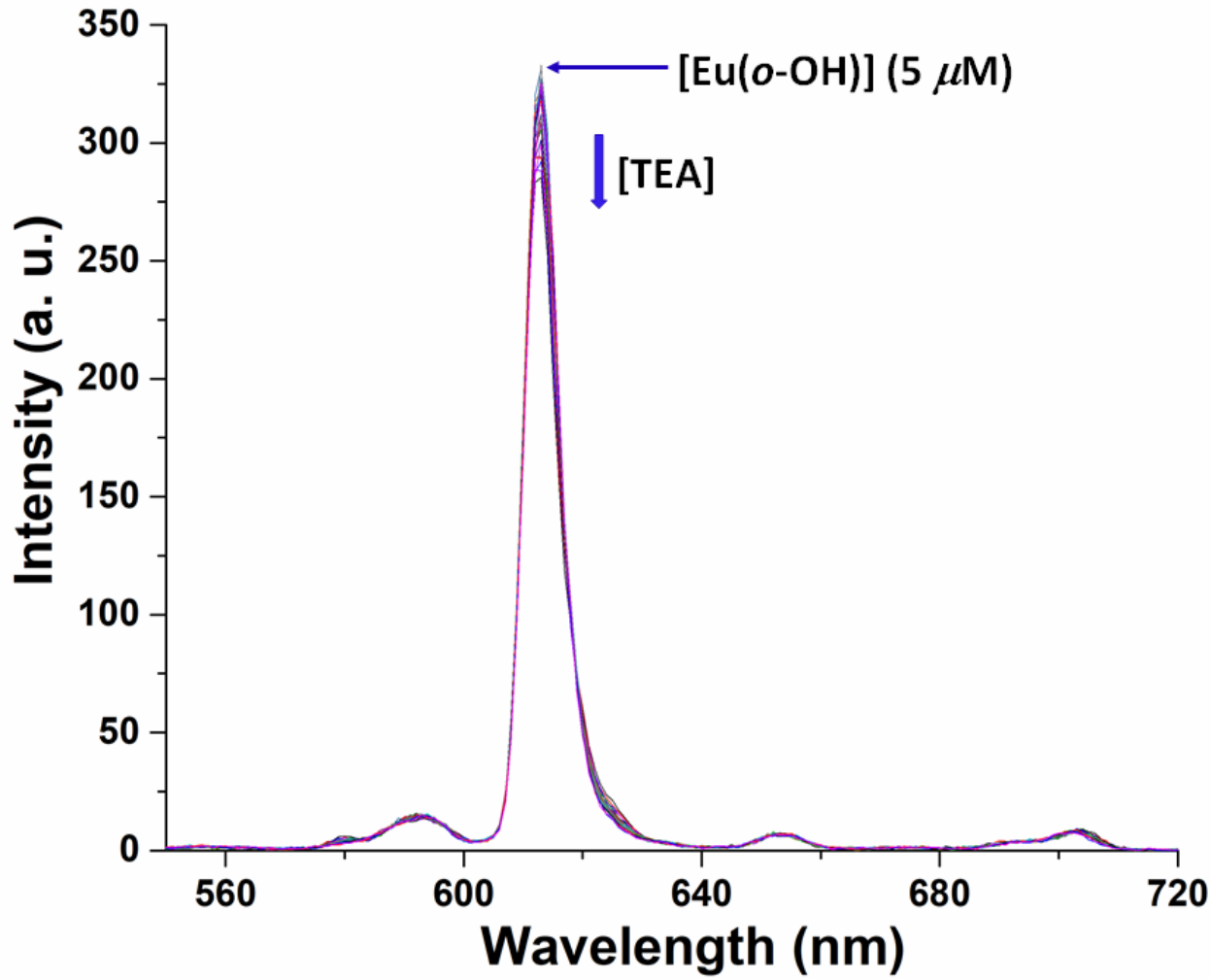

Figure S13. Changes in the PL spectra (λ_{ex} = 340 nm) of **Eu(*o*-OH)** (5 μM) with the increasing concentration of triethylamine (**TEA**) (0-50 μM) observed at characteristic emission from the hypersensitive band of Eu(III) ion ($^5D_0 \rightarrow {}^7F_2$ = 613 nm).

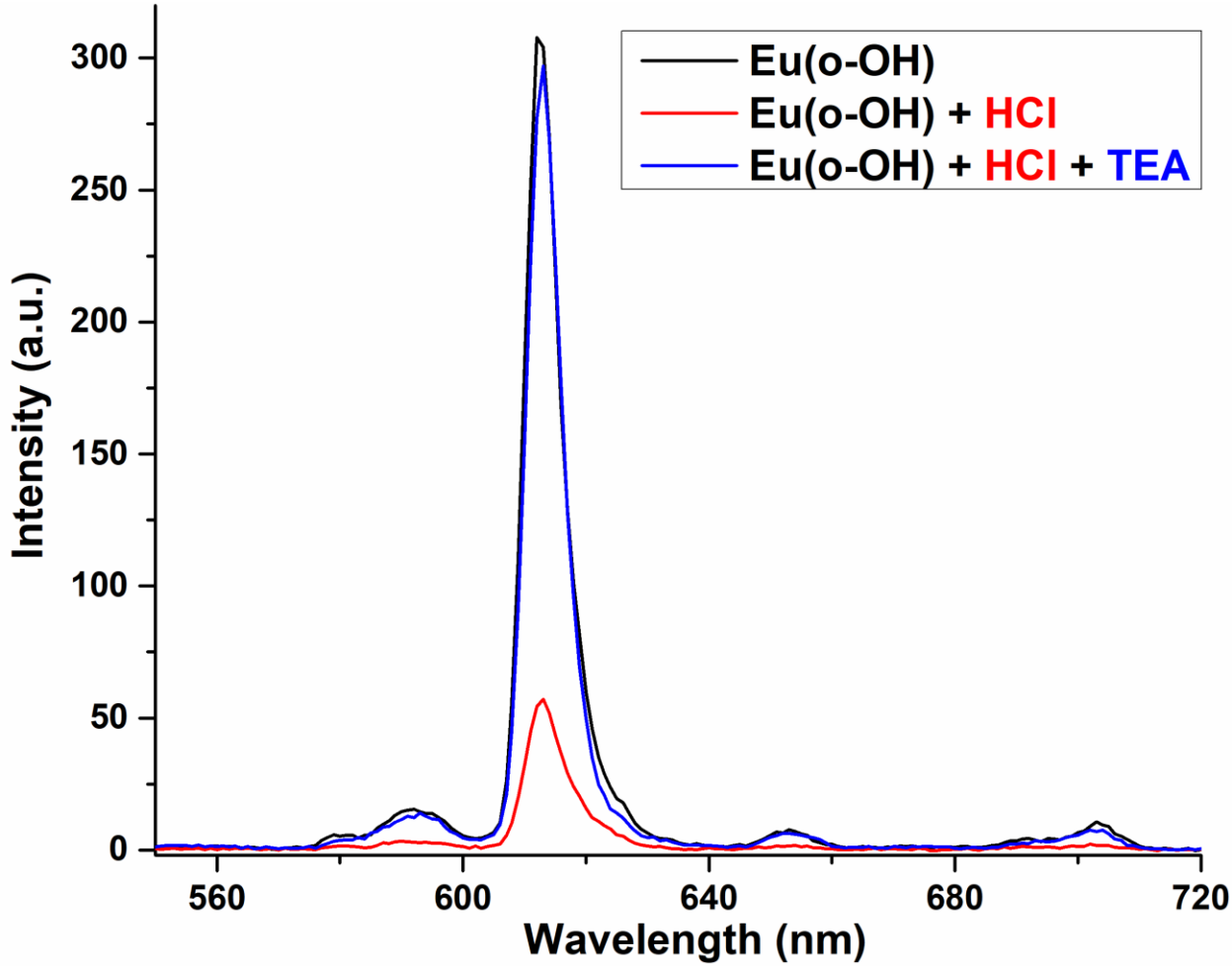

Figure S14. Reversible changes in the PL (λex = 340 nm) of **Eu(*o*-OH)** (5 μM) with the addition of **HCl** (0-30 μM) followed by the addition of **TEA** (0-30 μM) observed at characteristic emission from the hypersensitive band of Eu(III) ion ($^5D_0 \rightarrow {}^7F_2$ = 613 nm).

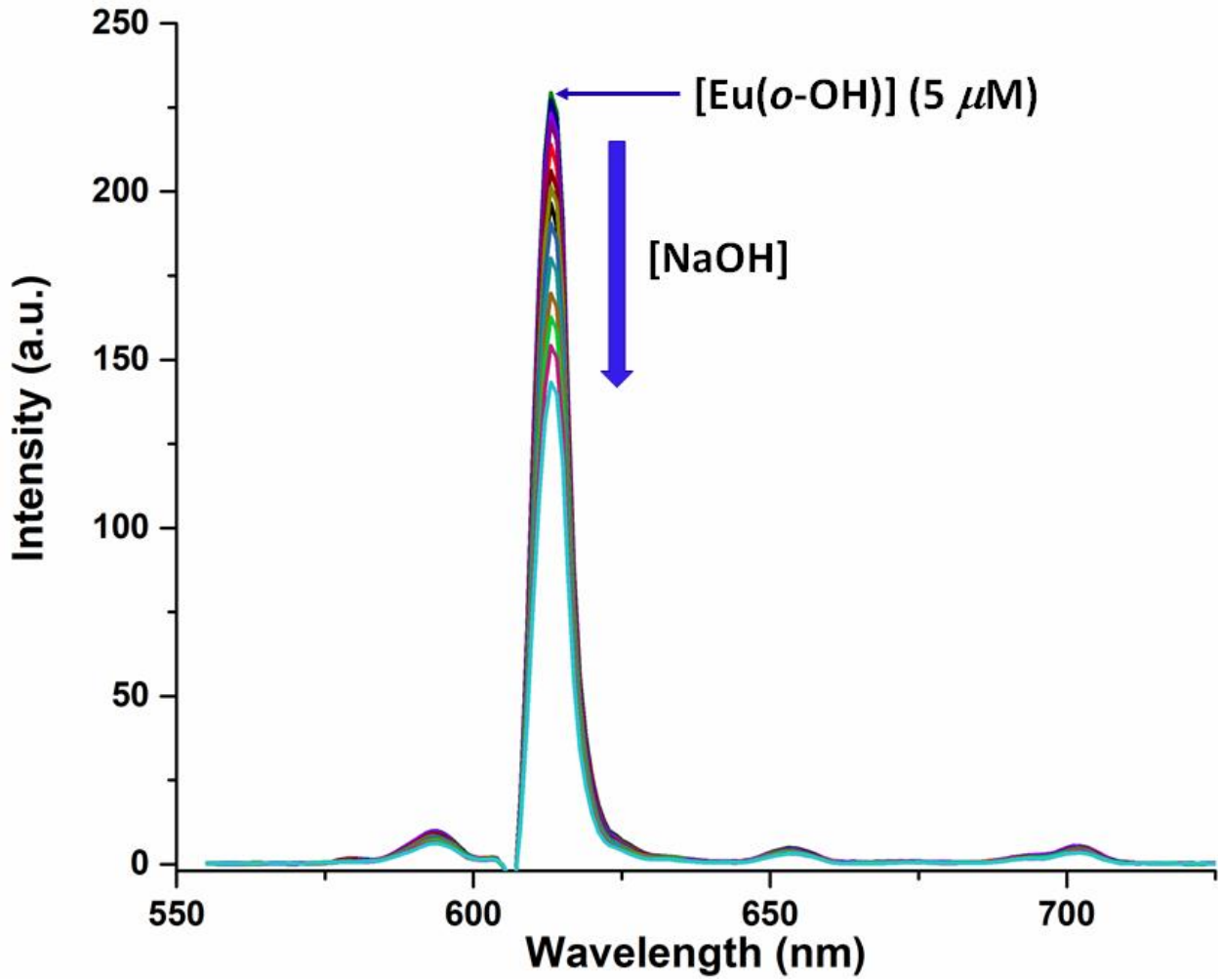

Figure S15. Changes in the PL spectra (λ_{ex} = 340 nm) of **Eu(*o*-OH)** (5 μM) with the increasing concentration of **NaOH** (0-7.5 μM) observed at characteristic emission from the hypersensitive band of Eu(III) ion ($^5D_0 \rightarrow {}^7F_2$ = 613 nm).

NMR titration studies of [La(*o*-HPIP)(TTA)$_3$] with DCP in DMSO-d6

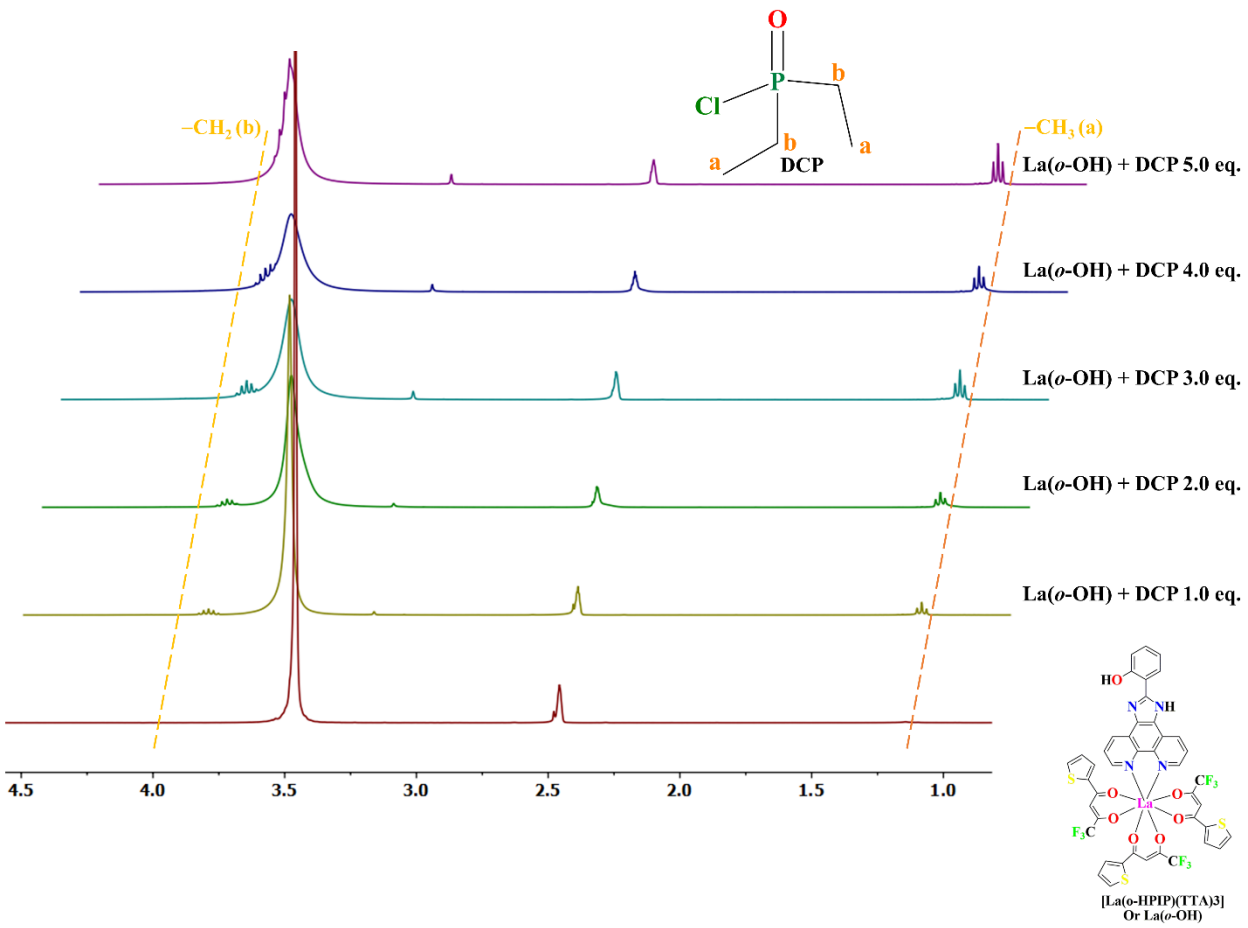

Figure S16. Overlaid ^{1}H-NMR signals of the **La(*o*-OH)** (20 mM) in the aliphatic region of the spectrum with the gradual addition of DCP (0-100 mM).

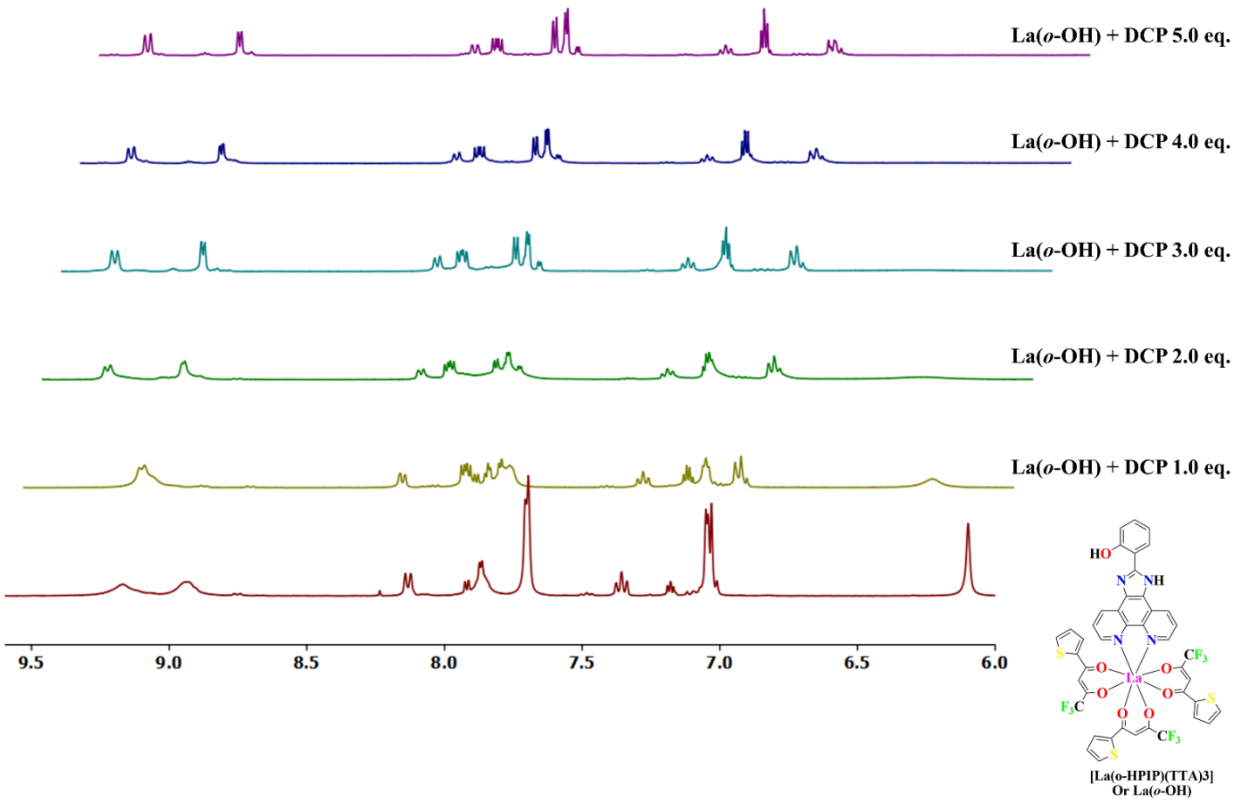

Figure S17. Overlaid ^{1}H-NMR signals of the **La(*o*-OH)** (20 mM) in the aromatic region of the spectrum with the gradual addition of DCP (0-100 mM).

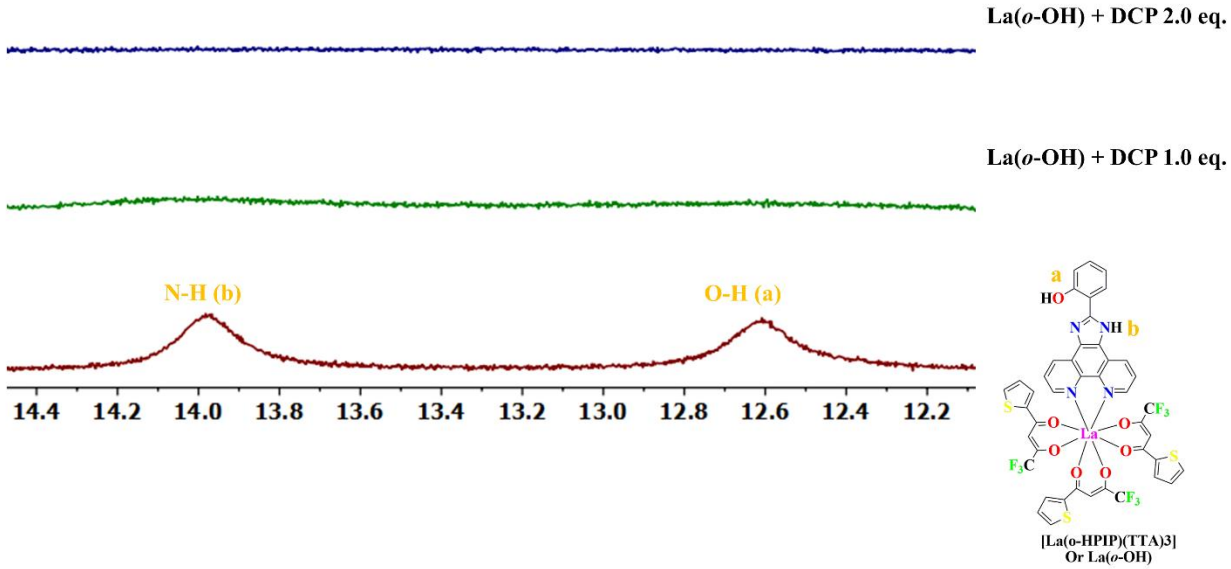

Figure S18. Overlaid ^{1}H-NMR signals of the **La(*o*-OH)** (20 mM) showing the broad signals corresponding to O-H and N-H proton disappears with gradual addition of DCP (0-40 mM) due to proposed phosphorylation reaction.

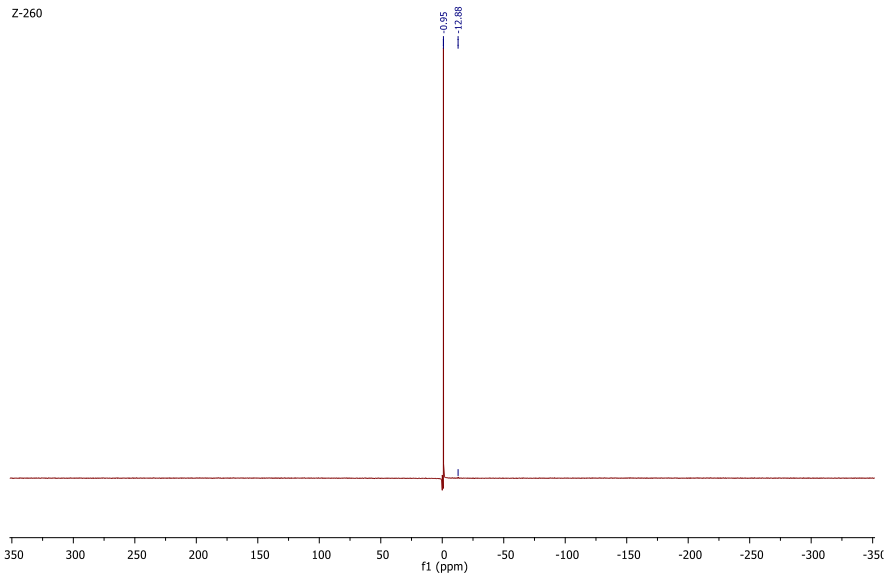

Figure S19. ^{31}P-NMR signals of the **La(*o*-OH)** (20 mM) showing a single sharp signal after the addition of DCP (100 mM).

Limit of Detection Calculations:

$$\mathbf{LOD = 3.3\sigma/s}$$

Where, $\boldsymbol{\sigma}$ is the standard deviation of the regression line and ***s*** is the slope of the curve.

For **Eu(*o*-OH)**, ***s*** = 0.3724 and $\boldsymbol{\sigma}$ = 0.0124

For **Eu(*p*-OH)**, ***s*** = 0.5442 and $\boldsymbol{\sigma}$ = 0.0092

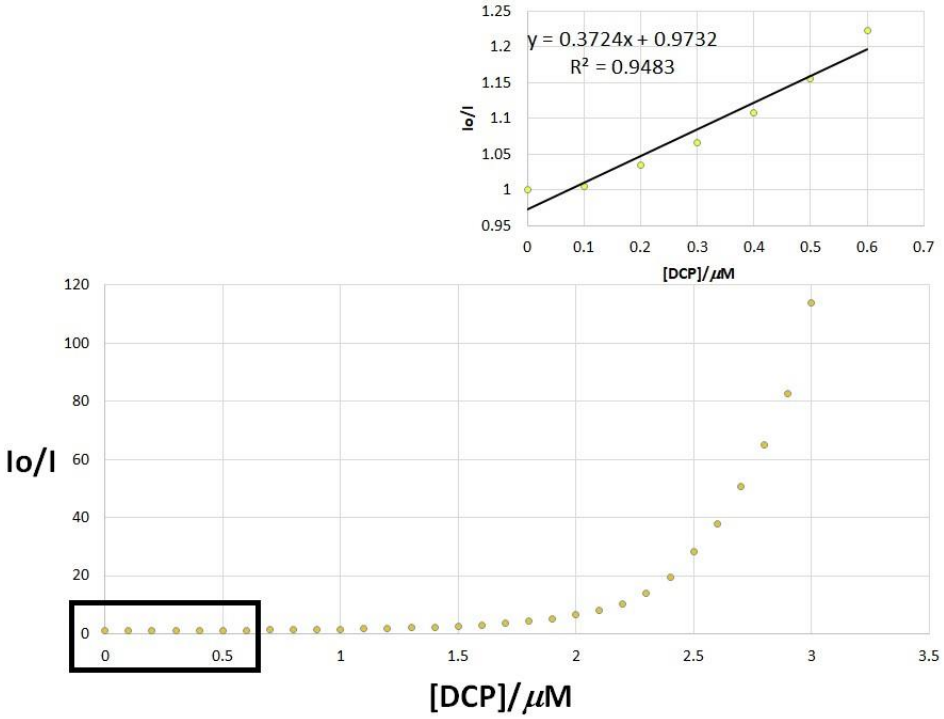

Figure S20. Representation of plot from the luminescence titration for the calculation of limit of detection (LOD) for DCP from the line of regression for **Eu(*o*-OH)** probe.

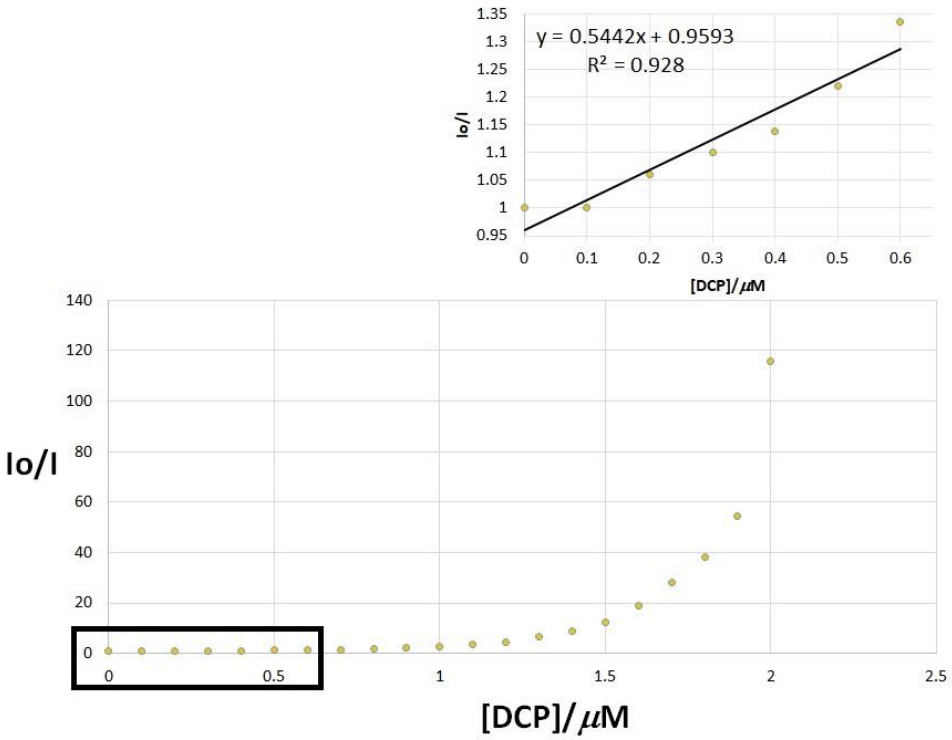

Figure S21. Representation of plot for the calculation from the luminescence titration for the calculation of limit of detection (LOD) from the line of regression for **Eu(*p*-OH)** probe.